Review

Electrochemical Reduction of Carbon Dioxide on Graphene-Based Catalysts

Stefan Delgado [ID], María del Carmen Arévalo, Elena Pastor *[ID] and Gonzalo García *[ID]

Instituto de Materiales y Nanotecnología, Departamento de Química, Universidad de La Laguna, P.O. Box 456, 38200 La Laguna, Santa Cruz de Tenerife, Spain; sdelgadb@ull.edu.es (S.D.); carevalo@ull.edu.es (M.d.C.A.)
* Correspondence: epastor@ull.edu.es (E.P.); ggarcia@ull.edu.es (G.G.)

Abstract: The current environmental situation requires taking actions regarding processes for energy production, thus promoting renewable energies, which must be complemented with the development of routes to reduce pollution, such as the capture and storage of CO_2. Graphene materials have been chosen for their unique properties to be used either as electrocatalyst or as catalyst support (mainly for non-noble metals) that develop adequate efficiencies for this reaction. This review focuses on comparing experimental and theoretical results of the electrochemical reduction reaction of carbon dioxide (ECO_2RR) described in the scientific literature to establish a correlation between them. This work aims to establish the state of the art on the electrochemical reduction of carbon dioxide on graphene-based catalysts.

Keywords: CO_2; graphene; HER; electrocatalysts; catalysis; Cu; nanoparticles

1. Introduction

Over the last few decades, the drastic increase of carbon dioxide into the atmosphere has caused global warming and the acidification of the oceans, among other environmental problems, thus leading to climate change. The accelerated consumption of fossil fuels has been the priority factor in these problems, but it has not only caused a crisis in the environmental field but also brought an energy crisis. This is a fact that also affects health because air pollution is the sixth-leading cause of death, causing over two million premature deaths worldwide in addition to increasing asthma, respiratory diseases, diseases cardiovascular disease, cancer, etc. [1]. To put an end to this environmental situation, the Paris Agreement, which aims to keep the global temperature rise below 2 °C by 2100 and limit the temperature increase to 1.5 °C above pre-industrial levels, was drawn up in 2015 [2].

For this, complementary strategies are needed to the transition towards renewable energies, including the capture and storage of CO_2, which help, together with natural processes (photosynthesis and underground mineralization), to balance the presence of CO_2 in the atmosphere [3]. Carbon capture and use (CCU) has arisen to reduce carbon emissions by using 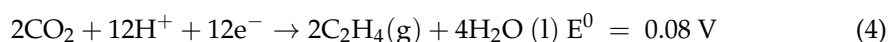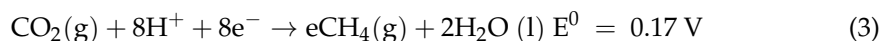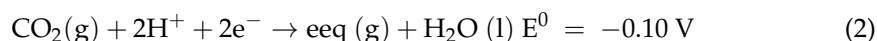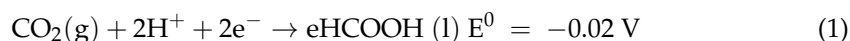CO_2 as a raw material. Some examples include the production of methanol, dimethyl carbonate, and sodium carbonate; however, not all of these are sustainable. In this regard, most of these processes require significant energy inputs that carry carbon footprints themselves. Due to these problems related to economic viability, it is difficult to analyze the sustainability of CCU technology [4].

Therefore, it is necessary to develop innovative strategies that are capable of converting carbon dioxide into products of energy value (e.g., hydrocarbons and alcohol), thus increasing its applications while reducing emissions. Among the possible conversion products, formic acid has been proposed as a suitable material for the combination of hydrogen storage and CO_2 fixation. This compound is easy to store and transport, can be used directly in direct formic acid fuel cells (DFAFCs), and releases H_2 at room temperature using suitable metal catalysts [5–7]. Other oxygenated products, such as methanol and

ethanol, are promising due to their high energy density, safety, and easy storage; additionally, like formic acid, they present the possibility of working directly in fuel cells. On the other hand, ethylene has enormous added value [8,9]. Of the different ways of converting CO_2, chemical, photochemical, and electrochemical reductions stand out. Specifically, the electrochemical reduction process has been extensively investigated in recent years [10].

CO_2 is a very stable molecule under environmental conditions, and its electrochemical reduction reaction (ECO_2RR) is an endothermic process that requires the participation of multiple electrons and protons. Furthermore, the reaction intermediates of the different stages form various products in turn, depending on the material used as cathode and the applied potential (reduction potential values for Equations (1)–(10) are given relative to a reversible hydrogen electrode (RHE) at pH 7, 1.0 atm, and 25 °C in aqueous solution) [11,12]. Due to this, the selectivity for the desired products is not usually very high, and it is also conditioned by the hydrogen evolution reaction (HER; $E^0 = 0.000$ V), which competes with the reaction under study. This currently raises the following challenges for the ECO_2RR: the need for an increased reaction efficiency, the need for a decreased overpotential to overcome energy barriers and suppress the HER, and the need to obtain moderately high current densities for commercial applications [13,14].

$$CO_2(g) + 2H^+ + 2e^- \rightarrow eHCOOH \ (l) \ E^0 \ = \ -0.02 \text{ V} \tag{1}$$

$$CO_2(g) + 2H^+ + 2e^- \rightarrow eeq \ (g) + H_2O \ (l) \ E^0 \ = \ -0.10 \text{ V} \tag{2}$$

$$CO_2(g) + 8H^+ + 8e^- \rightarrow eCH_4(g) + 2H_2O \ (l) \ E^0 \ = \ 0.17 \text{ V} \tag{3}$$

$$2CO_2 + 12H^+ + 12e^- \rightarrow 2C_2H_4(g) + 4H_2O \ (l) \ E^0 \ = \ 0.08 \text{ V} \tag{4}$$

$$CO_2(g) + 6H^+ + 6e^- \rightarrow eCH_3OH(l) + H_2O \ (l) \ E^0 \ = \ 0.02 \text{ V} \tag{5}$$

$$2CO_2(g) + 12H^+ + 12e^- \rightarrow 2C_2H_5OH(l) + 3H_2O \ (l) \ E^0 \ = \ 0.09 \text{ V} \tag{6}$$

$$CO_2(g) + 4H^+ + 4e^- \rightarrow eeq \ Eq(l) + H_2O \ (l) \ E^0 \ = \ -0.07 \text{ V} \tag{7}$$

$$2CO_2(g) + 2H^+ + 2e^- \rightarrow eH_2C_2O_4(l) \ E^0 \ = \ -0.50 \text{ V} \tag{8}$$

$$2CO_2 + 14H^+ + 14e^- \rightarrow 4C_2H_6(g) + 4H_2O \ (l) \ E^0 \ = \ 0.14 \text{ V} \tag{9}$$

$$CO_2(g) + e^- \rightarrow \ CO_2^{\bullet -} \ E^0 \ = \ -1.900 \text{ V} \tag{10}$$
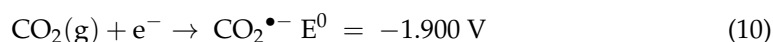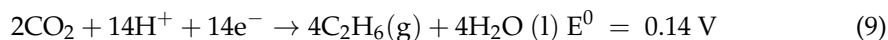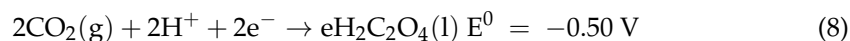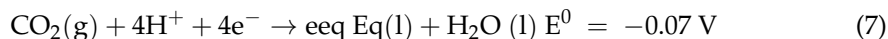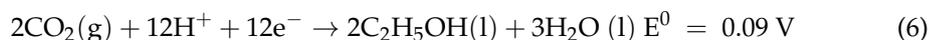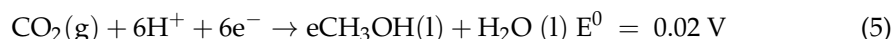
For these reasons, current research is focused on the development of electrocatalysts that are chemically stable and inexpensive, have an appropriate shelf life, have an adequate product selectivity to promote their formation, and (ultimately) have the ability to operate at industry-acceptable current densities [13,15]. Various catalysts have been developed to improve the energy efficiency of the electrochemical reduction of CO_2 with metals from the d-block (Cu, Co Pt, Fe, Au, Pd, Ag, Zn, Ni, etc.) and from the p-block (In, Sn, Pb, Bi, etc.) [10,16–20]. Specifically, Cu is a unique metallic catalyst for this reaction because it can efficiently reduce CO_2 to hydrocarbons and oxygenates such as alcohols (either methanol or ethanol), carbon monoxide, and formic acid/format [8,9,21].

However, in certain cases, excessive overpotentials are required and current densities are not very high. Additionally, for other reasons such as toxicity and the cost of metals, it is intended to develop catalysts without noble metals that can generate the products with acceptable efficiency and conditions [7,22–24]. To achieve these catalysts, carbon-based materials are being investigated with special interest due to their wide range of possible nanostructures and because they may adsorb hydrogen and suppress the HER at low overpotentials [25]. Among the wide variety of these materials, graphene (G) and graphene materials (GMs) have become particularly important. In terms of electrochemical activity, pristine graphene is not active for the CO_2 electroreduction. However, the electrocatalytic activity is enhanced after doping with oxygenated groups and other heteroatoms (Figure 1) [7,26]. Nitrogen was used with the first metal-free G-based catalyst for

the ECO$_2$RR, and it is the most widely used heteroatom [22,24,25], although there have been studies with others such as B [23], P [15], S [7], F, Cl, Br, and I [11].
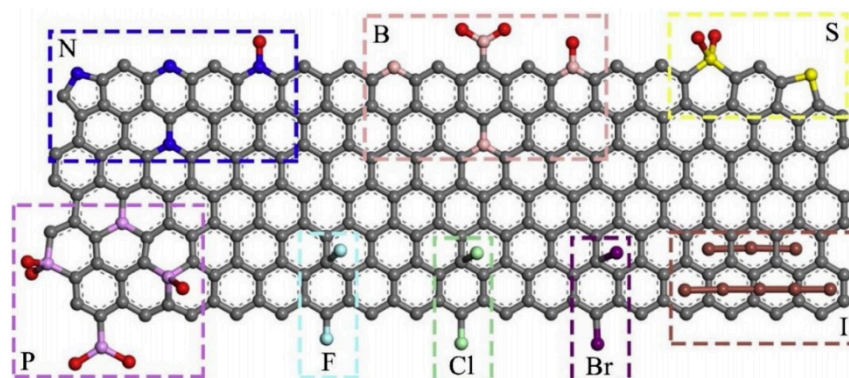

Figure 1. Different possibilities of heteroatom-doped graphene materials. Reproduced with permission [11].

Reaction Mechanism: Key Intermediates, Rate-Determining Steps and Products

The single electron reduction of CO$_2$ to a CO$_2$$^{\bullet-}$ radical occurs at E^0 = −1.90 V vs. RHE (Equation (10)) with a high energy contribution so that it accepts an electron, which causes the molecule to lose its initial linear structure and generate a bent radical anion. The lifetime of this radical is very short, thus making it difficult to clearly know its structure. Despite this, it has been established that, for Cu—which is the most studied metal (although it can be generalized for Ag and Au, given their similarity in terms of reaction kinetics and electronic properties)—the bond angle and the distance change, giving rise to the carboxylate intermediate η^2 (C,O)-CO$_2$$^{\bullet-}$ adsorbed on the metal surface [11,27–29].

Proton-coupled multi-electron steps for the ECO$_2$RR are generally more favorable than single electron reductions due to the more thermodynamically stable molecules that are produced (Equations (1)–(9)). Furthermore, these reactions are influenced by the pH of the electrolyte, and diverse species may therefore be promoted by a specific concentration of protons in the solution [30]. The species produced depend on the catalyst surface nature, e.g., if the CO$_2$ adsorption occurs trough carbon, OCHO* is obtained, but if it is trough oxygen, COOH* is formed (* represents an adsorbed species). Hydrogen adsorption and the HER may also occur at the same potential range than the ECO$_2$RR, and a competition between both reactions may consequently happen. Then, it is possible to reach a whole series of C$_1$ compounds such as HCOOH, HCHO, CH$_3$OH, and CH$_4$ through both routes. To produce C$_{2+}$ (hydrocarbons and oxygenate species, e.g., C$_2$H$_4$, C$_2$H$_6$, and C$_2$H$_5$OH), the coupling of C$_1$ intermediates is required so that a C–C bond is formed [27,28,31].

Another important adsorbed intermediate is *CO, which is the common species for most of the products that are subsequently generated because of its stability. Its protonation can occur trough carbon in order to generate CHO* or trough oxygen to obtain COH*, but the first option is more common. This protonation is one of the most important rate-determining steps [28]. It should be noted that a strong CO* bonding poisons the catalyst, and the HER is preferred. On the other hand, weak CO* adsorption can result in CO desorption, and the reduction will therefore not continue towards other C$_1$ products [13].

Figure 2 depicts two pathways to generate *CHO. One of them is through the following species: COOH*, CO*, and CHO*. The other one is through the following species: OCHO*, HCOOH* and CHO*. In this regard, thermodynamics dictate that OCHO* is more favorable than COOH*, although the latter has been more reported in the literature [27].
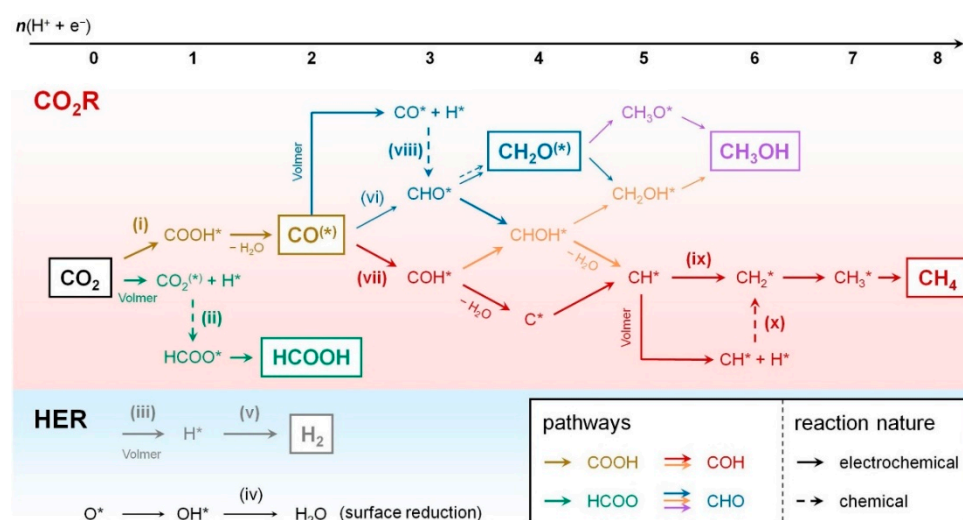
Figure 2. Scheme of the reaction pathways and key intermediates for different CO_2 electroreduction products. Reproduced with permission [32]. HER: hydrogen evolution reaction.

Another crucial anion that is formed as an intermediate is the dimer $(CO)_2{}^-$, which has a relevant role in the mechanisms for the formation of C_2 species. Proton transfer only occurs once the dimer has formed; consequently, dimer formation is the step that limits the rate of the reaction for the formation of these species with two C atoms [30].

2. Graphene-Based Catalysts

2.1. Metal-Free Graphene-Based Electrocatalysts

Most of the works reported in the literature have studied the ECO_2RR with graphene materials before preparing the composite with the metal, thus serving as a reference. In general, the ECO_2RR results of metal-free graphene materials are bad, and the efficiencies are low. Thus, in the work of Huang et al., partially-oxidized, 5-nm cobalt nanoparticles (PO-5 nm Co) dispersed on a single-layer nitrogen-doped graphene (SL-NG) (denoted as PO-5 nm Co/SL-NG) were synthesized and employed for the ECO_2RR [19]. SL-NG activity is even worse than for PO-Co, and only PO-Co/SL-NG is interesting due to the synergistic effect that occurs after its combination. Something similar was obtained in the work of Ning et al. with cuprous oxide supported on reduced graphene oxide (Cu_2O/rGO) and cuprous oxide supported on nitrogen-doped reduced graphene oxide (Cu_2O/N-rGO) [9]. The authors added additional information with data for rGO and N-rGO. The results were not good either because for both GMs, the main product was H_2. Because of these data, it can be concluded that these GMs are not active materials for the ECO_2RR, even after being doped with N [9].

Other studies have confirmed this fact [33–35]. In the work of Xiong et al. [34], Cu-Sn catalysts were supported on N-doped graphene (NG). For this material, the majority product in the ECO_2RR is H_2, and the faradaic efficiency (FE) for this gas reaches 79% at −1.0 V vs. RHE, while it decreases to 68% and 42%, respectively, for Cu/NG and Sn/NG following the previous trend that proves the low activity of GMs for the reaction under study [34]. Additionally, in the work of Hossain et al. [33], in which they deposited Cu nanoparticles (NPs) on rGO, the researchers showed that the catalytic activity of rGO is very similar to that of unsupported Cu NPs, both being very low (Figure 3).
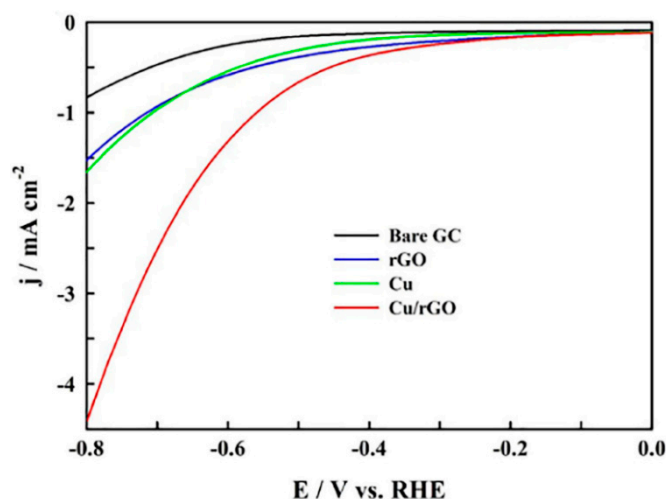
Figure 3. Linear sweep voltammogram (LSV) for glassy carbon (GC), rGO, Cu nanoparticles (NPs), and Cu/rGO in a 0.1 M NaHCO$_3$ solution at a scan rate of 20 mVs^{-1}. Reproduced with permission [33]. RHE: reversible hydrogen electrode.

Chen et al. developed a 2D/0D composite catalyst formed from bismuth oxide nanosheets and nitrogen-doped graphene quantum dots (Bi$_2$O$_3$-NGQDs) [35]. The electrochemical response of Bi$_2$O$_3$ and Bi$_2$O$_3$-NGQDs is shown in Figure 4 and is compared with that of the graphene material, NGQDs. By comparing the current densities and the FEs for formate production, it was found that the activity of the NGQDs is extremely low, with an FE of around 15%, while the Bi$_2$O$_3$ and Bi$_2$O$_3$-NGQD present FEs close to 85% and 100%, respectively, at a potential of -0.9 V (vs. RHE) [35].
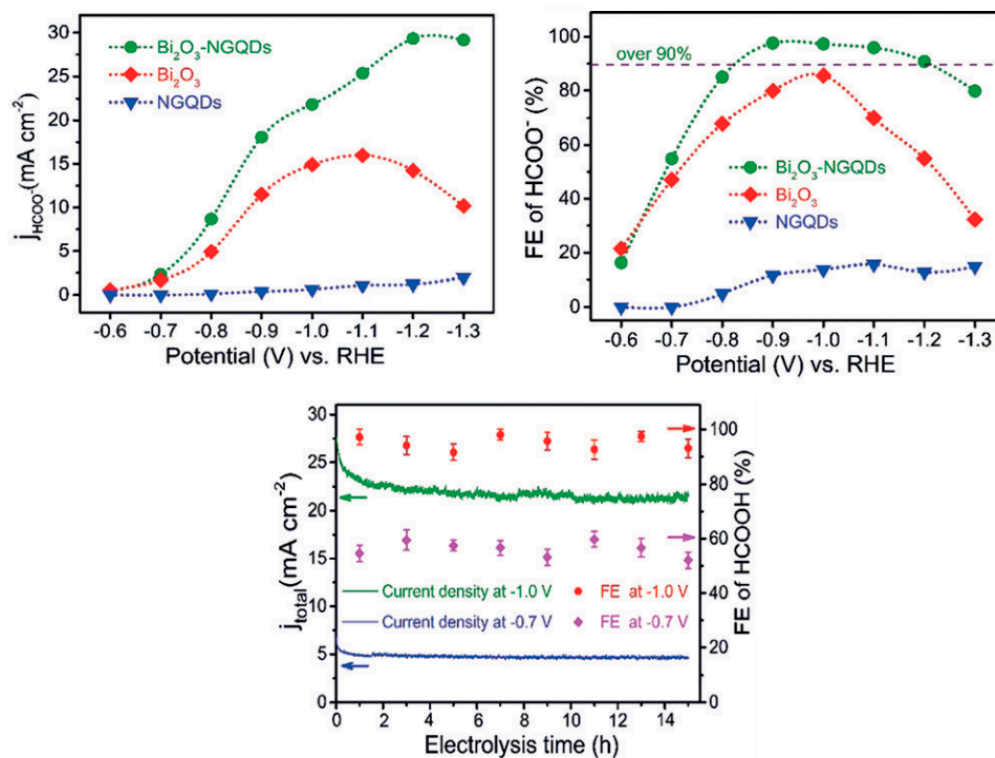

Figure 4. Faradaic efficiency (FE) and formate partial current density for Bi$_2$O$_3$-NGQD (nitrogen-doped graphene quantum dot), Bi$_2$O$_3$, and NGQD at different potentials (upper panels) and long-term electrolysis experiments of Bi$_2$O$_3$-NGQD recorded at -0.7 V and -1.0 V (bottom panel) in a 0.5 M KHCO$_3$ electrolyte. Reproduced with permission [35].

Despite the low activities shown in the works mentioned above, there are several strategies to design efficient metal-free electrocatalysts for the ECO$_2$RR. For instance, Wu et al. prepared NGQDs that exhibit a high total carbon dioxide reduction efficiency of up to 90%, with selectivity for conversions to ethylene and ethanol reaching 45% in 1 M KOH [36]. Furthermore, the amounts of C$_2$ and C$_3$ species produced are comparable to those of electrocatalysts based on Cu NPs. The great difference in the results employing similar materials may be related to the synthetic method, the pH, and the counterion, among other factors.

Other significant work is reported by Han and col. that prepared graphene (G), nitrogen-doped graphene (NG), edge-rich graphene (EG), and defective graphene (DG). DG was synthesized through the elimination of the nitrogen atoms from an NG structure, which caused many topological defects that offered abundant catalytically active sites, high electronic conductivity, and strong CO$_2$ adsorption [7]. This work revealed the great potential of DG as a metal-free GM for the ECO$_2$RR. DG exhibited an excellent FE of 84% for CO production at −0.6 V (vs. RHE), with a smaller overpotential and a higher electrocatalytic activity toward the ECO$_2$RR in comparison with the rest of materials (Figure 5).
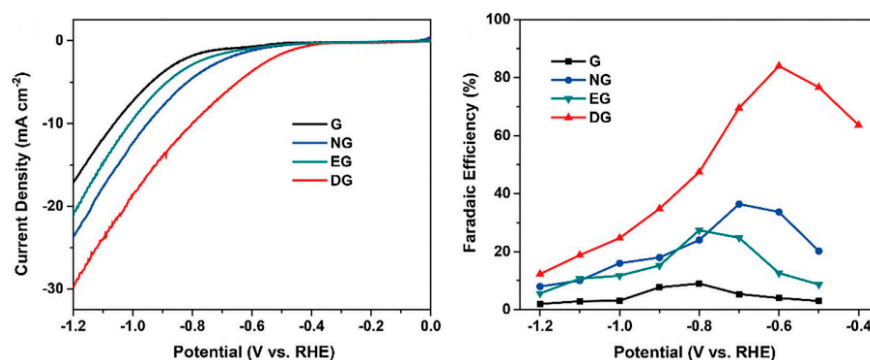

Figure 5. LSV curves in a 0.1 M KHCO$_3$ electrolyte (the scan rate was 10 mVs^{-1}) and faradaic efficiencies to CO at different applied potentials on pristine graphene, nitrogen-doped graphene (NG), edge-rich graphene (EG), and defective graphene (DG). Reproduced with permission [7].

Furthermore, the DG electrocatalyst was relatively stable after 10 h of the continuous ECO$_2$RR at −0.6 V (vs. RHE) (Figure 6a). In addition, Figure 6b reveals the operating mechanism and the best performance of the DG catalyst. Indeed, a Tafel slope value of 139 mV·dec^{-1} was obtained for DG, which indicates the initial electronic transfer to the adsorbed CO$_2$ molecule to form the intermediate CO$_2^{\bullet-}$ as the rate-determining step (RDS). The rest of the catalysts showed higher Tafel slope values that indicated the slower kinetics for the RDS [7].
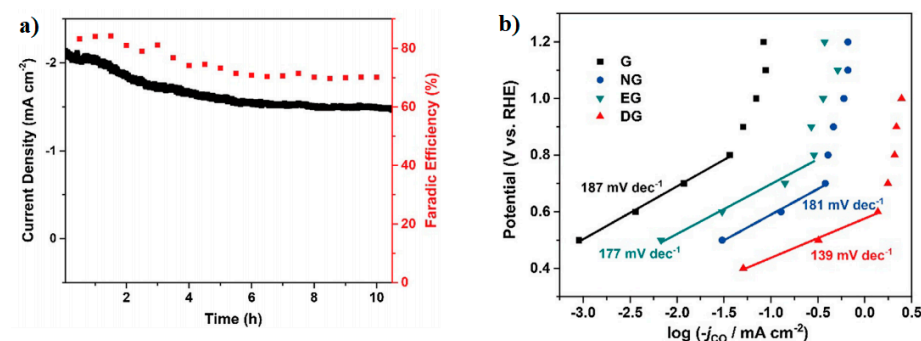

Figure 6. (**a**) Time-dependent total current density curve (left *y*-axis) and faradic efficiency for CO (right *y*-axis) at DG at −0.6 V (vs. RHE) in 0.1 M KHCO$_3$. (**b**) Tafel plots for all catalysts. Reproduced with permission [7].

2.2. Graphene-Supported Metal Nanoparticles

The results described in the bibliography show that each metal catalyst exhibits differences in terms of efficiency and selectivity to reduce CO_2 to different products. However, when graphene materials are used as metal support, there is a reduction in the free energy of the reaction in comparison with unsupported metal catalysts [16,18,27,37]. By applying DFT (density functional theory) calculations, Lin et al. showed that the interaction with graphene produces a strong influence on the formation of COOH* and CHO* species, as well as the suppression of HCOOH (Figure 7) [18]. With a higher Fermi level than CO_2 molecules, the upper graphene layer injects electrons into the nonbonding orbitals of COOH* and CHO*, resulting in charge redistribution and electrostatic interaction between the molecules and graphene. The last reduces the free energies of the reaction and the onset potentials of crucial reaction steps (Figure 7b). Figure 7a shows the decrease in the free energy due to the incorporation of graphene; the reaction is consequently more thermodynamically favorable for both pathways (COOH* and CHO*), with the effect on the production of hydrocarbons being more significant in comparison with HCOOH [18]. Interestingly, these theoretical results have been confirmed with experimental studies [9,38].
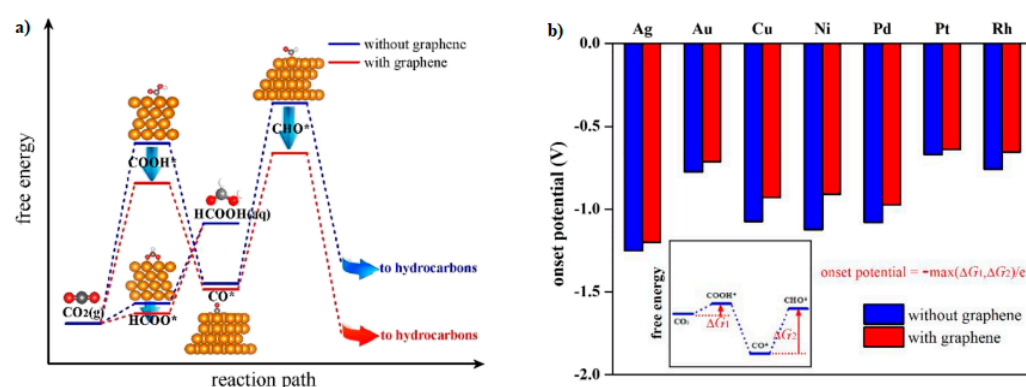

Figure 7. (**a**) A schematic free energy diagram. (**b**) Onset potentials for the electrochemical reduction reaction of carbon dioxide (ECO_2RR) on metal surfaces with and without a graphene overlayer. Reproduced with permission [18].

Hossain et al. designed an easy procedure to synthesize a nanostructured thin film comprising NPs of Cu on rGO obtained by the direct electrochemical reduction of a mixture of copper and GO precursors [33]. The Cu (NP)/rGO film exhibited excellent stability and catalytic activity for the electrochemical reduction of CO_2 in an aqueous solution, almost tripling the current densities in comparison with unsupported Cu NPs (Figure 3). Carbon monoxide and formate were found as the main products by chromatography, and the achieved FE was close to 69% at −0.6 V (vs. RHE, reference hydrogen electrode) [33]. On the other hand, nanocubes of cuprous oxide (Cu_2O) incorporated into rGO and Cu_2O (rGO) revealed promising results [9]. Figure 8a,b compare the FEs achieved at glassy carbon-supported Cu_2O and Cu_2O/rGO, respectively. The main outcomes indicated that the incorporation of the graphene material raised the production of CO and H_2 and increased the stability of Cu_2O nanocubes.

The incorporation of a second metal has been considered in theoretical calculations [31,39]. In order to modulate the interaction between the bimetallic catalyst and the graphene-based support (and therefore modify the catalytic activity), Cu, Ni, Pd, Pt, Ag, and Au were combined and compared with monometallic dimers by calculation [31]. It was found that Pt_2, AgNi, Pd_2, and AgPt supported on defective graphene revealed the lowest overpotential values for the ECO_2RR [31]. On the other hand, transition metal dimers (Cu_2, CuMn, and CuNi) introduced into single graphene vacancies (called @ 2SV) were studied for the ECO_2RR by DFT [39]. All samples revealed a low overpotential, a high FE, and selectivity for species production during the ECO_2RR. In this regard, Cu_2 @ 2SV, MnCu @ 2SV, and NiCu @ 2SV promoted the formation

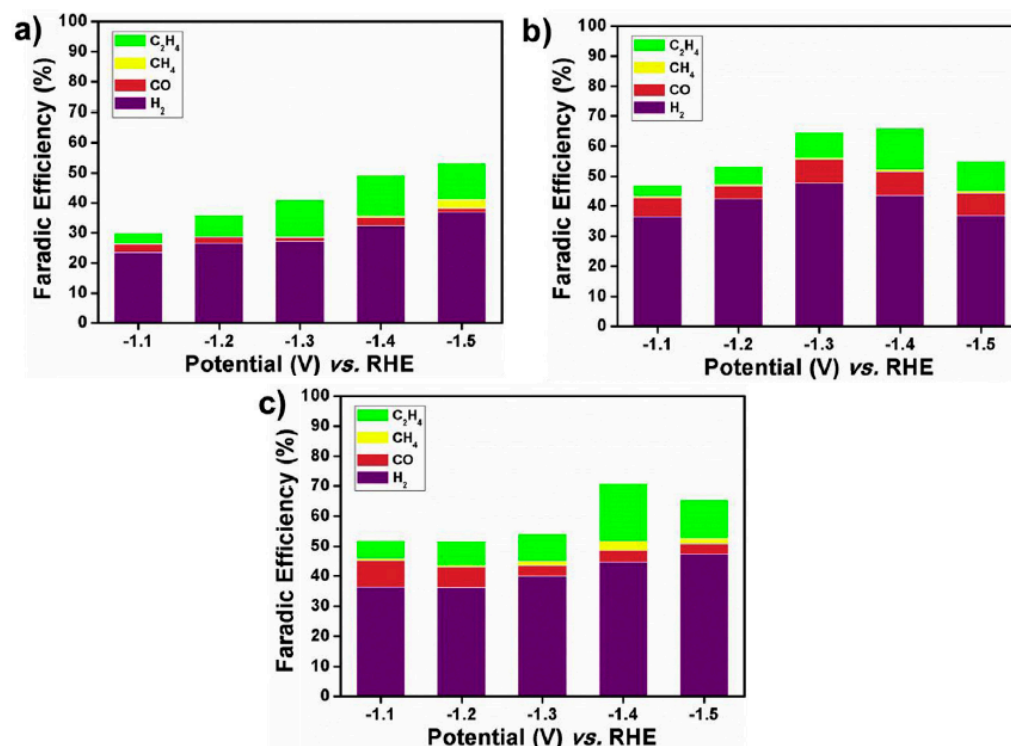of CO, CH$_4$, and CH$_3$OH, respectively. Results were explained in terms of the oxophilicity of Ni and Mn [39].

Figure 8. Faradaic efficiency of the gas products for (**a**) Cu$_2$O, (**b**) Cu$_2$O/rGO, and (**c**) Cu$_2$O/N-rGO in a 0.1 M KHCO$_3$ solution. Reproduced with permission [9].

Bimetallic catalysts have also been employed in experimental studies. For instance, Pd-Cu/graphene catalysts with diverse Pd-Cu wt% ratios were synthesized from graphite oxide suspensions and metal precursor salts by applying the sodium borohydride reduction method [38]. Particle sizes ranging from 8 to 10 nm were acquired, and the best catalytic performance toward the ECO$_2$RR was achieved with 1 wt% Pd–2 wt% Cu/graphene material [38].

In addition to copper-based catalysts, WC [13], Bi [17], In$_2$O$_3$ [37], and Pd-In [40] materials were supported on GMs, and a good catalytic performance toward the ECO$_2$RR has been accomplished. For instance, three-dimensional Pd/graphene (Pd/3D-rGO), In/3D-rGO, and Pd-In/3D-rGO catalysts were prepared by a mild method that combined chemical and hydrothermal steps [40]. 3D-rGO materials are 3D structures with a high density of interconnected pores and metal NPs anchored on the folds. Interestingly, Pd$_{0.5}$-In$_{0.5}$/3D-rGO showed the smallest particle size, and its dispersion on rGO sheets was found to be more homogeneous than monometallic catalysts of Pd and In. These characteristics enhance the performance for the ECO$_2$RR, decreasing the overpotential and increasing the FE to 85.3% at −1.6 V (vs. Ag/AgCl) in 0.5 M KHCO$_3$ for formate production [40].

2.3. Metal Nanoparticles Supported on Heteroatom-Doped Graphene Materials

The introduction of heteroatoms into the graphene structure may improve the catalytic activity towards the ECO$_2$RR. For example, Figure 8c shows that Cu$_2$O supported on N-doped rGO (Cu$_2$O/N-rGO) enhances the FE up to 70%, raises the production of ethylene at −1.4 V (vs. RHE), and increases the catalytic stability. Based on these results, the authors concluded that pyridine nitrogen improves the catalytic stability of Cu$_2$O due to N (pyridine)–Cu interactions [9].

CuSn alloy nanoparticles supported on an NG material stand out due to their low cost and unique catalytic activities towards the ECO$_2$RR. Nitrogen doping into graphene

sheets results in the strong binding of CuSn NPs to the catalyst support. The strong binding prevents alloy NP detachment and agglomeration, thereby improving the long-term stability. Furthermore, electron transfer from NG to CuSn NPs appears to be beneficial for the adsorption of CO_2 and/or hydrogen, thus enhancing the CO_2RR performance [34].

Figure 9 depicts the distribution of products generated during this reaction as a function of the applied potential for different copper–tin ratios on NG, and an optimal composition was obtained for Cu-$Sn_{0.175}$. This alloy generated C_1 products with an FE close to 93% at −1.0 V (vs. RHE), which was the highest of all prepared materials. This led to considerable improvements over Cu and Sn separately, which were found to develop FEs of 32% and 58%, respectively [34]. To clarify the experimental results, DFT simulations of the free energy for hydrogen adsorption and CO_2 reduction were carried out (Figure 10). The main results indicated that hydrogen can be easily adsorbed on Sn surfaces, but the free energies become higher after Cu introduction, and the HER is accordingly suppressed. After that, more H atoms can participate in the ECO_2RR processes [34].
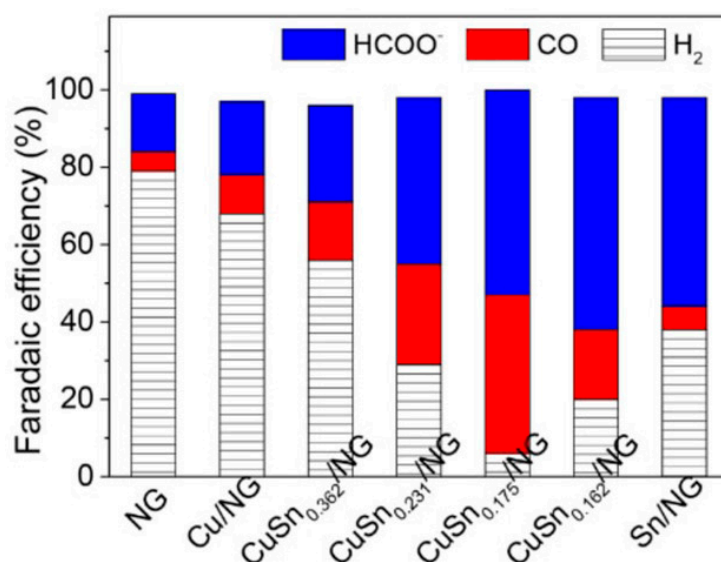
Figure 9. Faradaic efficiency of Cu-Sn NPs on NG with various ratios of Cu to Sn at −1.0 V (vs. RHE) for the ECO_2RR (0.5 M $KHCO_3$). Reproduced with permission [34].
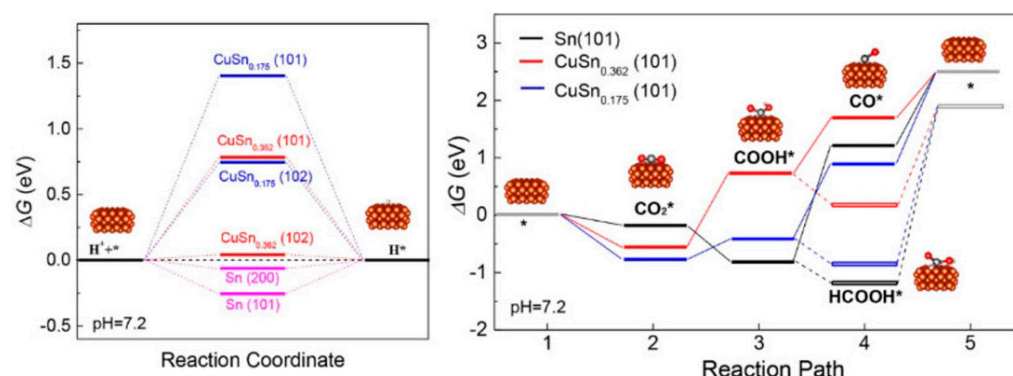
Figure 10. Left panel: Schematic Gibbs free energy profile for the H adsorption on different surfaces. Right panel: schematic Gibbs free energy profile for the detailed CO_2RR pathway on the surface (101) of three models. Reproduced with permission [34].

On the other hand, Figure 11a illustrates the synergy between the catalyst and the catalyst support as an important increment of the faradaic current discerned at PO-5 nm Co/SL-NG catalyst. Additionally, the catalyst revealed remarkable stability, even after 10 h of CO_2 electrolysis, both in current and in morphology, particle size, structure, and

metal content, with an FE above 70% at −0.90 V (vs. SCE (saturated calomel electrode)) for methanol production (Figure 11b) [19].
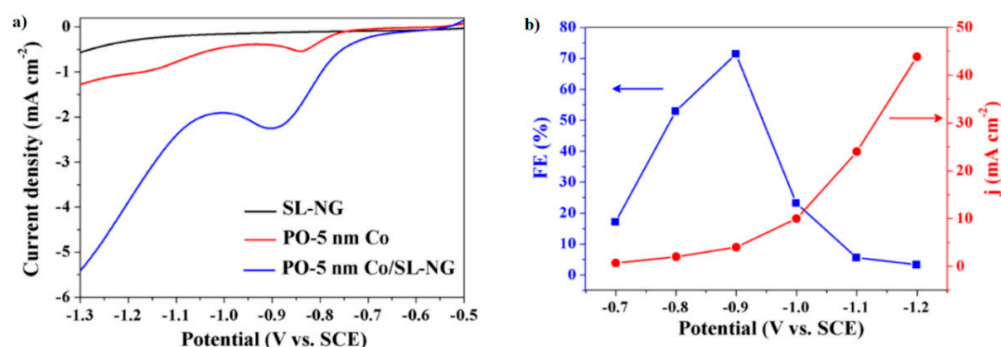

Figure 11. (**a**) Linear sweep voltammograms of single-layer nitrogen-doped graphene (SL-NG), 5-nm cobalt nanoparticles (PO-5 nm Co) and PO-5 nm Co/SL-NG in 0.1 M $NaHCO_3$ at 20 mV s^{-1}. (**b**) FE of methanol and current density for PO-5 nm Co/SL-NG under various electrolysis potentials for 10 h. Reproduced with permission [19].

As stated above, Chen et al. developed a 2D/0D composite catalyst formed by Bi_2O_3-NGQDs [34]. This material exhibits an FE of almost 100% for formate production with a moderate potential of −1.0 V (vs. RHE) and good stability (Figure 4). Results were attributed through DFT calculations to an increment of the adsorption energy of CO_2 and OCHO* after the combination of Bi_2O_3 with NGQDs (Figure 12b). Figure 12a illustrates the free energy diagram for the HCOOH formation process on Bi_2O_3 and Bi_2O_3-NGQDs materials, which reveals the highest energy barrier for the OCHO* formation that intensely falls for Bi_2O_3-NGQDs. Furthermore, the energy barrier for the HER increases for MG, thus explaining the preference of Bi_2O_3-NGQDs material to generate formate over H_2 [35].
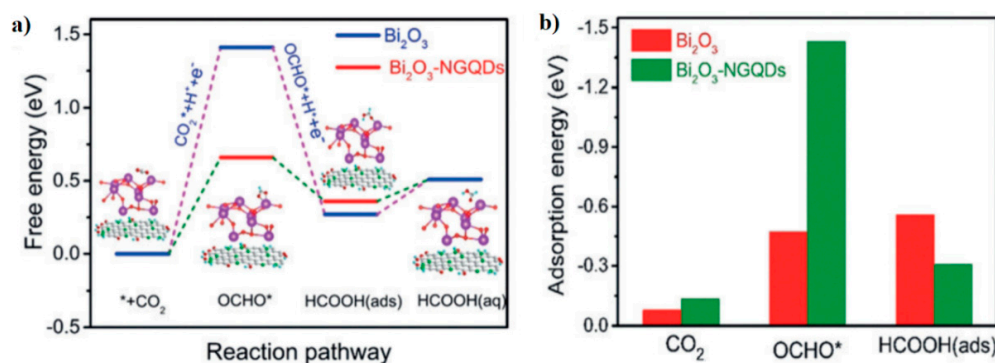

Figure 12. (**a**) Free-energy diagram and (**b**) adsorption energy of CO_2, OCHO*, and HCOOH (ads) for Bi_2O_3 and Bi_2O_3-NGQDs. Reproduced with permission [35].

3. Perspective

In this review, the general concept of the CO_2 reduction reaction was discussed, with special attention paid to low temperature electrolysis with graphene-based electrode materials.

The conversion of CO_2 to chemicals usable as fuels via room temperature electrolysis with graphene-based catalysts is a very attractive technology for energy conversion and storage. This technology has the potential to reduce the produced CO_2 through its conversion into valuable energy carriers (hydrocarbons, alcohols, or CO-rich feeds) that will help to improve environmental contamination.

With the aim to solve the principal catalytic problem at the cathodes of low temperature electrolyzers, the fundamental study of carbon dioxide, as well as hydrogen evolution on graphene-based materials in a wide pH range, was considered.

In general, the results discussed in this manuscript confirm that graphene materials are excellent supports, producing synergistic effects that cause improvements in the efficiency and selectivity of the catalysts used for the electrochemical reduction of CO_2. However, in most cases, the activity of graphene not modified by metal species is very low. All the new advances in the fundamental understanding of reactions occurring on graphene-based catalysts presented here may help to improve the fabrication of novel electrodes in order to enhance the performance and decrease the cost of this technology.

Conflicts of Interest: The authors declare no conflict of interest.

References

1. Jacobson, M.Z. Review of solutions to global warming, air pollution, and energy security. *Energy Environ. Sci.* **2008**, *2*, 148–173. [CrossRef]
2. Ollila, A. Challenging the scientific basis of the Paris climate agreement. *Int. J. Clim. Chang. Strat. Manag.* **2019**, *11*, 18–34. [CrossRef]
3. Wang, Q.; Tao, L.; Jiang, X.; Wang, M.; Shen, Y. Graphene oxide wrapped $CH_3NH_3PbBr_3$ perovskite quantum dots hybrid for photoelectrochemical CO_2 reduction in organic solvents. *Appl. Surf. Sci.* **2019**, *465*, 607–613. [CrossRef]
4. Roh, K.; Lim, H.; Chung, W.; Oh, J.; Yoo, H.; Al-Hunaidy, A.S.; Imran, H.; Lee, J.H. Sustainability analysis of CO_2 capture and utilization processes using a computer-aided tool. *J. CO_2 Util.* **2018**, *26*, 60–69. [CrossRef]
5. Choi, J.; Wagner, P.; Gambhir, S.; Jalili, R.; Macfarlane, D.R.; Wallace, G.G.; Officer, D.L. Steric modification of a cobalt phthalocyanine/graphene catalyst to give enhanced and stable electrochemical CO_2 reduction to CO. *ACS Energy Lett.* **2019**, *4*, 666–672. [CrossRef]
6. Wu, S.-Y.; Chen, H.-T. CO_2 Electrochemical reduction catalyzed by graphene supported palladium cluster: A computational guideline. *ACS Appl. Energy Mater.* **2019**, *2*, 1544–1552. [CrossRef]
7. Han, P.; Yu, X.; Yuan, D.; Kuang, M.; Wang, Y.; Al-Enizi, A.M.; Zheng, G. Defective graphene for electrocatalytic CO_2 reduction. *J. Colloid Interface Sci.* **2019**, *534*, 332–337. [CrossRef]
8. Yuan, J.; Yang, M.-P.; Zhi, W.-Y.; Wang, H.; Wang, H.; Lu, J.-X. Efficient electrochemical reduction of CO_2 to ethanol on Cu nanoparticles decorated on N-doped graphene oxide catalysts. *J. CO_2 Util.* **2019**, *33*, 452–460. [CrossRef]
9. Ning, H.; Mao, Q.; Wang, W.; Yang, Z.; Wang, X.; Zhao, Q.; Tian, X.; Wu, M. N-doped reduced graphene oxide supported Cu_2O nanocubes as high active catalyst for CO_2 electroreduction to C_2H_4. *J. Alloys Compd.* **2019**, *785*, 7–12. [CrossRef]
10. Yang, Y. Electrocatalytic reduction of CO_2 on mono-metal/graphene/polyurethane sponge electrodes. *Int. J. Electrochem. Sci.* **2019**, *14*, 3805–3823. [CrossRef]
11. Ma, T.; Fan, Q.; Li, X.; Qiu, J.; Wu, T.; Sun, Z. Graphene-based materials for electrochemical CO_2 reduction. *J. CO_2 Util.* **2019**, *30*, 168–182. [CrossRef]
12. Fan, Q.; Ma, T.; Tao, H.; Fan, Q.; Han, B. Fundamentals and challenges of electrochemical CO_2 reduction using two-dimensional materials. *Chem* **2017**, *3*, 560–587. [CrossRef]
13. Ananthaneni, S.; Smith, Z.; Rankin, R.B. Graphene supported tungsten carbide as catalyst for electrochemical reduction of CO_2. *Catalysts* **2019**, *9*, 604. [CrossRef]
14. Huang, Q.; Liu, H.; An, W.; Wang, Y.; Feng, Y.; Men, Y. Synergy of a metallic NiCo dimer anchored on a C_2N–graphene matrix promotes the electrochemical CO_2 reduction reaction. *ACS Sustain. Chem. Eng.* **2019**, *7*, 19113–19121. [CrossRef]
15. Zhi, X.; Jiao, Y.; Zheng, Y.; Qiao, S. Impact of interfacial electron transfer on electrochemical CO_2 reduction on graphitic carbon nitride/doped graphene. *Small* **2019**, *15*, e1804224. [CrossRef]
16. Nguyen, D.L.T.; Lee, C.W.; Na, J.; Kim, M.-C.; Tu, N.D.K.; Lee, S.Y.; Sa, Y.J.; Won, D.H.; Oh, H.-S.; Kim, H.; et al. Mass transport control by surface graphene oxide for selective CO production from electrochemical CO_2 reduction. *ACS Catal.* **2020**, *10*, 3222–3231. [CrossRef]
17. Wu, D.; Chen, W.; Wang, X.; Fu, X.-Z.; Luo, J.-L. Metal-support interaction enhanced electrochemical reduction of CO_2 to formate between graphene and Bi nanoparticles. *J. CO_2 Util.* **2020**, *37*, 353–359. [CrossRef]
18. Lin, Z.-Z.; Chen, X.; Yin, C.; Yue, L.; Meng, F. Electrochemical CO_2 reduction in confined space: Enhanced activity of metal catalysts by graphene overlayer. *Int. J. Energy Res.* **2019**, *44*, 784–794. [CrossRef]

19.　Huang, J.; Guo, X.; Yue, G.; Hu, Q.; Wang, L. Boosting CH_3OH production in electrocatalytic CO_2 reduction over partially oxidized 5 nm cobalt nanoparticles dispersed on single-layer nitrogen-doped graphene. *ACS Appl. Mater. Interfaces* **2018**, *10*, 44403–44414. [CrossRef]

20.　Fu, Y.; Wang, T.; Zheng, W.; Lei, C.; Yang, B.; Chen, J.; Li, Z.; Lei, L.; Yuan, C.; Hou, Y. Nanoconfined tin oxide within N-doped nanocarbon supported on electrochemically exfoliated graphene for efficient electroreduction of CO_2 to formate and C_1 products. *ACS Appl. Mater. Interfaces* **2020**, *12*, 16178–16185. [CrossRef]

21.　Ni, W.; Li, C.; Zang, X.; Xu, M.; Huo, S.; Liu, M.; Yang, Z.; Yan, Y. Efficient electrocatalytic reduction of CO_2 on Cu_xO decorated graphene oxides: An insight into the role of multivalent Cu in selectivity and durability. *Appl. Catal. B Environ.* **2019**, *259*, 118044. [CrossRef]

22.　Zou, X.; Liu, M.; Wu, J.; Ajayan, P.M.; Li, J.; Liu, B.; Yakobson, B.I. How nitrogen-doped graphene quantum dots catalyze electroreduction of CO_2 to hydrocarbons and oxygenates. *ACS Catal.* **2017**, *7*, 6245–6250. [CrossRef]

23.　Yuan, J.; Zhi, W.-Y.; Liu, L.; Yang, M.-P.; Wang, H.; Lu, J.-X. Electrochemical reduction of CO_2 at metal-free N-functionalized graphene oxide electrodes. *Electrochim. Acta* **2018**, *282*, 694–701. [CrossRef]

24.　Chai, G.-L.; Guo, Z.X. Highly effective sites and selectivity of nitrogen-doped graphene/CNT catalysts for CO_2 electrochemical reduction. *Chem. Sci.* **2016**, *7*, 1268–1275. [CrossRef]

25.　Siahrostami, S.; Jiang, K.; Karamad, M.; Chan, K.; Wang, H.; Nørskov, J. Theoretical investigations into defected graphene for electrochemical reduction of CO_2. *ACS Sustain. Chem. Eng.* **2017**, *5*, 11080–11085. [CrossRef]

26.　Chen, J.G.; Zhang, H.; Chen, J.G.; Lu, Q.; Cheng, M.-J. Constant electrode potential quantum mechanical study of CO_2 electrochemical reduction catalyzed by N-doped graphene. *ACS Catal.* **2019**, *9*, 8197–8207. [CrossRef]

27.　He, H.; Jagvaral, Y. Electrochemical reduction of CO_2 on graphene supported transition metals—Towards single atom catalysts. *Phys. Chem. Chem. Phys.* **2017**, *19*, 11436–11446. [CrossRef]

28.　Cui, X.; An, W.; Liu, X.; Wang, H.; Men, Y.; Wang, J. C_2N-graphene supported single-atom catalysts for CO_2 electrochemical reduction reaction: Mechanistic insight and catalyst screening. *Nanoscale* **2018**, *10*, 15262–15272. [CrossRef]

29.　Chernyshova, I.V.; Somasundaran, P.; Ponnurangam, S. On the origin of the elusive first intermediate of CO_2 electroreduction. *Proc. Natl. Acad. Sci. USA* **2018**, *115*, E9261–E9270. [CrossRef]

30.　Kortlever, R.; Shen, J.; Schouten, K.J.P.; Calle-Vallejo, F.; Koper, M.T.M. Catalysts and reaction pathways for the electrochemical reduction of carbon dioxide. *J. Phys. Chem. Lett.* **2015**, *6*, 4073–4082. [CrossRef]

31.　He, H.; Morrissey, C.; Curtiss, L.; Zapol, P. Graphene-supported monometallic and bimetallic dimers for electrochemical CO_2 reduction. *J. Phys. Chem. C* **2018**, *122*, 28629–28636. [CrossRef]

32.　Tang, M.; Peng, H.; Lamoureux, P.; Bajdich, M.; Abild-Pedersen, F. From electricity to fuels: Descriptors for C_1 selectivity in electrochemical CO_2 reduction. *Appl. Catal. B Environ.* **2020**, *279*, 119384. [CrossRef]

33.　Hossain, M.N.; Wen, J.; Konda, S.K.; Govindhan, M.; Chen, A. Electrochemical and FTIR spectroscopic study of CO_2 reduction at a nanostructured Cu/reduced graphene oxide thin film. *Electrochem. Commun.* **2017**, *82*, 16–20. [CrossRef]

34.　Xiong, W.; Yang, J.; Shuai, L.; Hou, Y.; Qiu, M.; Li, X.; Leung, M. CuSn alloy nanoparticles on nitrogen-doped graphene for electrocatalytic CO_2 reduction. *ChemElectroChem* **2019**, *6*, 5951–5957. [CrossRef]

35.　Chen, Z.; Mou, K.; Wang, X.; Liu, L. Nitrogen-doped graphene quantum dots enhance the activity of Bi_2O_3 nanosheets for electrochemical reduction of CO_2 in a wide negative potential region. *Angew. Chem. Int. Ed.* **2018**, *57*, 12790–12794. [CrossRef]

36.　Wu, J.; Ma, S.; Sun, J.; Gold, J.I.; Tiwary, C.; Kim, B.; Zhu, L.; Chopra, N.; Odeh, I.N.; Vajtai, R.; et al. A metal-free electrocatalyst for carbon dioxide reduction to multi-carbon hydrocarbons and oxygenates. *Nat. Commun.* **2016**, *7*, 13869. [CrossRef]

37.　Zhang, Z.; Ahmad, F.; Zhao, W.; Yan, W.; Zhang, W.; Huang, H.; Ma, C.; Zeng, J. Enhanced electrocatalytic reduction of CO_2 via chemical coupling between indium oxide and reduced graphene oxide. *Nano Lett.* **2019**, *19*, 4029–4034. [CrossRef] [PubMed]

38.　Liu, X.; Zhu, L.; Wang, H.; He, G.; Bian, Z. Catalysis performance comparison for electrochemical reduction of CO_2 on Pd–Cu/graphene catalyst. *RSC Adv.* **2016**, *6*, 38380–38387. [CrossRef]

39.　Li, Y.; Su, H.; Chan, S.H.; Sun, Q. CO_2 Electroreduction performance of transition metal dimers supported on graphene: A theoretical study. *ACS Catal.* **2015**, *5*, 6658–6664. [CrossRef]

40.　He, G.; Tang, H.; Wang, H.; Bian, Z. Highly selective and active Pd-In/three-dimensional graphene with special structure for electroreduction CO_2 to formate. *Electroanalysis* **2018**, *30*, 84–93. [CrossRef]